Climate variability in the SW Indian Ocean from an 8000-yr long multi-proxy record in the Mauritian lowlands shows a middle to late Holocene shift from negative IOD-state to ENSO-state

de Boer, E.J.; Tjallingii, R.; Vélez, M.I.; Rijsdijk, K.F.; Vlug, A.; Reichart, G.J.; Prendergast, A.L.; de Louw, P.G.B.; Vincent Florens, F.B.; Baider, C.; Hooghiemstra, H.

DOI
10.1016/j.quascirev.2013.12.026

Publication date
2014

Document Version
Final published version

Published in
Quaternary Science Reviews

Quaternary Science Reviews 86 (2014) 175–189

Contents lists available at ScienceDirect

Quaternary Science Reviews

journal homepage: www.elsevier.com/locate/quascirev

Climate variability in the SW Indian Ocean from an 8000-yr long multi-proxy record in the Mauritian lowlands shows a middle to late Holocene shift from negative IOD-state to ENSO-state

Erik J. de Boer [a,*], Rik Tjallingii [b], Maria I. Vélez [c], Kenneth F. Rijsdijk [d], Anouk Vlug [d], Gert-Jan Reichart [b], Amy L. Prendergast [e], Perry G.B. de Louw [f], F.B. Vincent Florens [g], Cláudia Baider [h], Henry Hooghiemstra [a]

[a] Department of Paleoecology and Landscape Ecology, Institute for Biodiversity and Ecosystem Dynamics, University of Amsterdam, Science Park 904, 1098 XH Amsterdam, The Netherlands
[b] Department of Marine Geology, Royal Netherlands Institute for Sea Research (NIOZ), PO Box 59, 1790 AB Den Burg, The Netherlands
[c] Department of Geology, University of Regina, Regina, Saskatchewan S4S 0A2, Canada
[d] Computational GeoEcology Department, Institute for Biodiversity and Ecosystem Dynamics, University of Amsterdam, Science Park 904, 1098 XH Amsterdam, The Netherlands
[e] Department of Archaeology and Anthropology, University of Cambridge, Downing Street, Cambridge CB13DZ, UK
[f] Deltares, PO Box 85467, 3584 CB Utrecht, The Netherlands
[g] Department of Biosciences, University of Mauritius, Réduit, Mauritius
[h] The Mauritius Herbarium, Agricultural Services, Ministry of Agro-Industry and Food Security, Réduit, Mauritius

ARTICLE INFO

Article history:
Received 31 July 2013
Received in revised form
20 December 2013
Accepted 21 December 2013
Available online 22 January 2014

Keywords:
Oceanic island
Sea level rise
Monsoon precipitation
Indian Ocean Dipole
El Niño-Southern Oscillation
Palm woodland
Semi-dry lowland forest

ABSTRACT

A multi-proxy reconstruction of a sediment core from the Tatos basin in the Mauritian lowlands reveals a dynamic environmental history during the last 8000 years. Under influence of sea level rise, the basin progressed from a wetland to a shallow lake between 8000 and 2500 cal yr BP and it slowly changed back into a wetland after sea level reached its highest position at around 2500 cal yr BP. The groundwater level in the basin was strongly affected by sea level rise and precipitation-forced runoff through the porous volcanic bedrock.

Millennial-scale precipitation changes in the Mauritian lowlands were derived from the pollen records of semi-dry forest and palm woodland. Salinity and environmental reconstructions based on diatoms, ostracods, stable isotopes and sediment composition showed numerous decadal and centennial droughts and wet events. Mauritius experienced wet conditions between ~8000 and ~6800 cal yr BP, followed by decreasing humidity from 6800 to 6000 cal yr BP. Dry conditions persisted until ~1200 cal yr BP, after which wetter conditions have prevailed as recorded from Mauritian lowland and upland records. Climate dynamics reflects northern hemisphere monsoon activity and suggest that Mauritian rainfall and the Indian and Asian summer monsoons are linked, as both receive moisture from the southern equatorial Indian Ocean.

The anti-phased relationship of climate dynamics between the Mauritian lowlands and western tropical Australia during the middle Holocene is interpreted as a prolonged configuration of a negative mode of the Indian Ocean Dipole (IOD). A negative IOD-like state is supported by decreased Asian summer monsoon rainfall, higher Austral-Indonesian summer monsoon rainfall and lower temperatures in the Kilimanjaro record. Conversely, repeated decadal-scale wet events in the Mauritian lowlands occurring every ~350 years reflect short positive IOD-like events.

The onset of ENSO climate variability followed an anomalously strong negative IOD-like event and shifted teleconnections from the tropical Indian Ocean to the Pacific Ocean. A shift in ENSO activity around ~2600 cal yr BP signifies the decoupling of ENSO from the Atlantic ITCZ. Subsequently, the influence of ENSO on climate in the western Indian Ocean is indicated by increased storm frequency and drought events after 2660 cal yr BP in Mauritius and reduced monsoon activity in the western and eastern Indian Ocean.

* Corresponding author.
E-mail address: e.j.deboer@uva.nl (E.J. de Boer).

0277-3791/$ – see front matter © 2013 Elsevier Ltd. All rights reserved.
http://dx.doi.org/10.1016/j.quascirev.2013.12.026

1. Introduction

Climate variability over the western Indian Ocean results from changes in the precession-driven northeast and southwest monsoons (Clemens and Prell, 2007), higher-frequent fluctuations of the Indian Ocean Dipole (IOD) and the El Nino-Southern Oscillation (ENSO) (e.g. Saji et al., 1999; Abram et al., 2007; Schott et al., 2009). Variations in the IOD and ENSO have been linked to variations in sea surface temperatures (SST), and interact significantly with each other (Schott and McCreary, 2001; Abram et al., 2009; Schefuß et al., 2011; Tierney et al., 2011). However, the history of the interactions and feedbacks of these major climate systems, SST, and precipitation is still uncertain.

Holocene climate of the western Indian Ocean and adjacent land masses have mainly been reconstructed from proxy records collected in a range of areas including East-African lakes (Vincens et al., 1993, 2005; Castañeda et al., 2009; Thomas et al., 2009; Verschuren et al., 2009; Berke et al., 2012), the Arabian Sea (Gupta et al., 2005; Fleitmann et al., 2007; Van Rampelbergh et al., 2013) and Madagascar (Gasse, 2000). These studies show a negative correlation between regions situated north and south of the equator, which are affected by the southwest and northeast monsoon respectively. Holocene climatic records reveal that the gradual southward migration of the Asian-African monsoon driven by precession, was interrupted by abrupt climatic events related with northern hemisphere cold events (Tierney et al., 2008; Verschuren et al., 2009; Schefuß et al., 2011). However, reconstructions of sub-millennial changes in the western Indian Ocean south of the equator are rare (Gasse and Van Campo, 1998; Burney et al., 2004; Virah-Sawmy et al., 2010; De Boer et al., 2013a). Detailed terrestrial archives that record Holocene environmental conditions east of Madagascar can provide insights on climatic variability in the western Indian Ocean.

In this study, we reconstruct Holocene environmental change from a sediment core from Tatos wetland, a small basin located 1.2 km from the current coastline. The island of Mauritius (20°18′ S, 57°35′ E) is situated at the extreme south end coverage of the annual cycle of the of the intertropical convergence zone (ITCZ) (Senapathi et al., 2010), which is a pivotal location to record meridional precipitation shifts. In addition, the oceanic island setting allows for a unique integration of terrestrial and marine climate records, as coastal island ecosystems are predominantly affected by external oceanic dynamics with little effect of the hinterland.

2. Regional setting

2.1. Geology and hydrology

Mauritius is a volcanic island located ~900 km east of Madagascar in the SW Indian Ocean (Fig 1). Mauritius (1865 km^2) comprises of several peaks reaching up to 828 m elevation and a central flat upland area between 500 and 650 m elevation that slopes gently towards the lowlands at the northern and eastern coastlines.

Tatos basin is situated in the eastern coastal lowlands and was formed after a phreatomagmatic explosion, probably during the youngest phase of volcanic activity between 700,000 and 20,000 years ago (Fig. 1). The basalts from this youngest series of lava outflows are highly permeable (Saddul, 2002) and therefore most of the precipitation is drained by a subsurface flow of groundwater. Fresh groundwater from higher grounds and catchments supplies a continuous flow of freshwater that emerges at coastal basins such as Tatos and Plance, which increase immediately after strong rainfall events (Rijsdijk et al., 2011).

2.2. Climate

Precipitation in the western Indian Ocean is mainly controlled by the African and Indian monsoon systems, which can be separated into northern and southern hemisphere components. The southwest monsoon, which is divided into the Indian summer monsoon (ISM) and Asian summer monsoon (ASM), prevails during the boreal summer whereas the northeast monsoon prevails during the austral summer (Van Rampelbergh et al., 2013). Recent data show that the southern equatorial Indian Ocean is the dominant source of moisture to the southwest monsoon, which results by cross-equatorial moisture transport (Clemens et al., 2010 and references therein). Due to its location in the southern equatorial Indian Ocean, paleomonsoon records from Mauritius are linked through a common moisture source with paleomonsoon records from the ISM and ASM systems (Rohling et al., 2009; Clemens et al., 2010).

Mauritius receives most of its precipitation from November to April brought by the northeast monsoon, and has a relative dry season from May to October under the influence of cool and dry easterly trade winds (Senapathi et al., 2010). Mean annual precipitation (MAP) depends on altitude and the orientation of the slopes with respect to the prevailing wind direction. The western coastal lowlands are relatively dry with an MAP of 800 mm (Padya, 1989). The MAP is about 1200 mm in the eastern coastal lowlands, and increases to more than 4000 mm at the elevated central part of the island. The mean annual evapotranspiration (MAE) in the coastal regions (<50 m elevation) exceeds MAP. Tatos is located at the windward position of the eastern coast, where the MAE is ~2200 mm and the MAP ~1300 mm.

The westbound South Equatorial Current flows along Mauritius all year round (Schott and McCreary, 2001; Schott et al., 2009). This current flows from the Indo-Pacific warm pool to the western equatorial Indian Ocean and is partially fed by warm, low salinity Pacific water through the Indonesian through flow (Gordon et al., 1997).

2.3. Coastal-lowland vegetation

About 95% of Mauritius has been deforested and an outline of the natural vegetation distribution must therefore rely on early historical records and small remnants of degraded natural vegetation. The pristine island was fringed by a variety of coastal vegetation communities such as mangroves, coastal marshes, coastal forest and vegetation associations characteristic of basaltic cliffs and coralline sand dunes (Cheke and Hume, 2008). On the driest parts of the island (MAP < 1000 mm), palm woodland occurred behind a strip of coastal vegetation (Cheke and Hume, 2008). In lowland areas where MAP range between 1000 and 1500 mm, semi-dry forest including ebony (*Diospyros*) forest, grew further inland behind the palm woodland or coastal vegetation (Vaughan and Wiehe, 1937; Cheke and Hume, 2008). Semi-dry forest was the dominant biome in the lowlands and covered over 40% of the island up to the start of human colonization in AD 1638 (Cheke and Hume, 2008). The island became rapidly deforested (Vaughan and Wiehe, 1937); the eastern lowland forests were largely destroyed in the 19th century. By AD 1872, palm-rich woodland had disappeared from the Mauritius main island (Safford, 1997; Cheke and Hume, 2008). The lowlands around Tatos basin were cleared between AD 1807 and 1835 (Vaughan and Wiehe, 1937) and converted into agricultural land (predominantly sugarcane). A botanical survey of Tatos wetland in 2008 by Baider and Florens identified 11 angiosperm species growing in the center, of which seven are native and four introduced (Bosser et al., 1976-onwards), and 37 angiosperm and

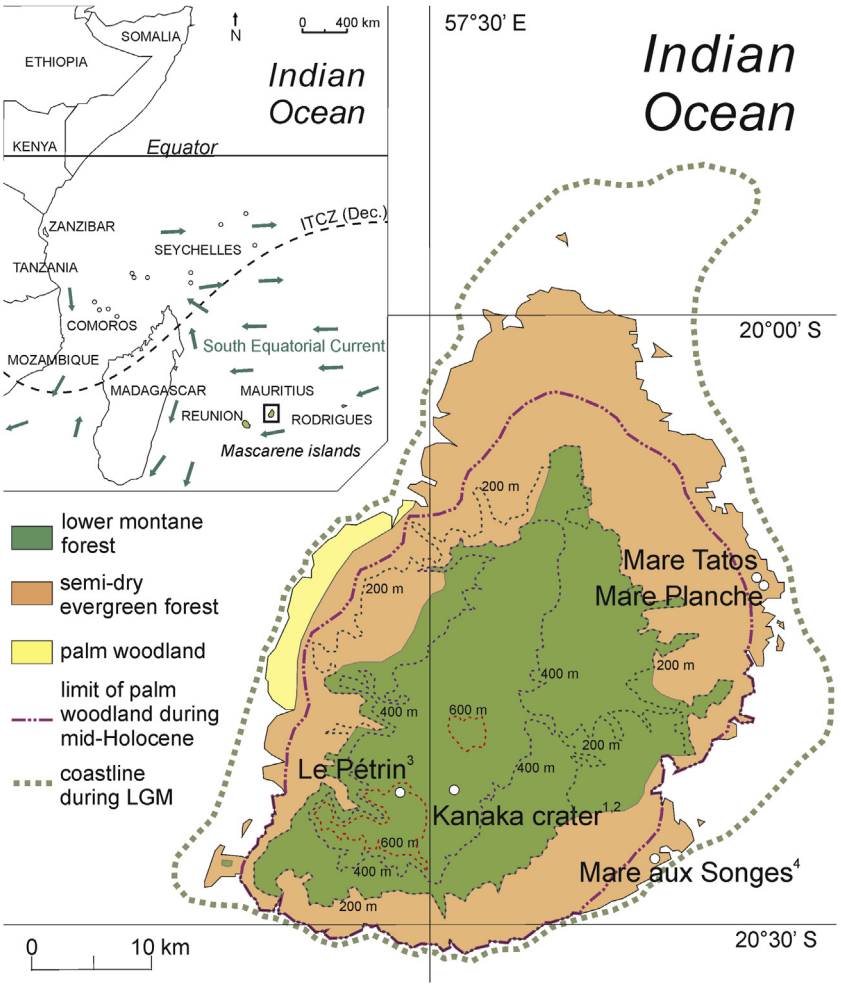

Fig. 1. Map of Mauritius showing the approximate coastline during the Last Glacial Maximum (−115 m), altitude lines (200 m steps), the distribution of main vegetation types before colonization (derived from Cheke and Hume, 2008) and the extension of palm woodland according to our results (this paper). The category 'lower montane forest' includes mid-altitude forest, moist forest, wet forest and azonal upland vegetation types (e.g. heath). Coastal forest, mangroves and wetlands are not shown. White dots indicate study areas discussed in the text. Green arrows in the inset shows the prevailing ocean currents in the Southwest Indian Ocean. [1]De Boer et al., 2013b [2]Van der Plas et al., 2012 [3]De Boer et al., 2013a [4]Rijsdijk et al., 2011. (For interpretation of the references to colour in this figure legend, the reader is referred to the web version of this article.)

fern species growing at the borders, of which 14 are native and 23 introduced (Bosser et al., 1976-onwards). Along the borders of the basin, species consisted mainly of exotic shrubs and herbs, but native lianas, shrubs and herbaceous plants (e.g. *Urera*, *Cissus*, *Dracaena*, *Hilsenbergia*, *Premna* and *Commelina*) and trees (*Ficus rubra*, *F. reflexa*, *Cassine*) were also found. These species are remnants of semi-dry forest. The wetland itself is currently filled with peat and consists mainly of native wetland species, such as grasses (Poaceae), *Typha*, mangrove fern *Acrostichum* and the vine species *Cassytha filiformis*.

3. Materials and methods

3.1. Core description and chronology

Sediment thickness in the wetland was measured along a transect with a 10 mm diameter fiberglass rod (Fig. 2), from which the longest coring location was selected. A 735-cm long core was retrieved using a Russian Corer (Ø 75 mm) in 50 cm increments until the rock basement was reached. Visual core description obtained directly after core recovery revealed a prominent peat layer situated at the base of the core, which gradually grades into siliciclastic sediments. Fine dark to light brown laminations were observed at several intervals. At 68 cm depth there is an abrupt transition from siliciclastic to peaty sediment.

The age model of the sediment core is based on 16 accelerator mass spectrometry (AMS) radiocarbon ages from seeds and other selected macrofossils. The southern hemisphere calibration curve (McCormac et al., 2004) was used to convert radiocarbon ages into calibrated calendar ages in years before present (cal yr BP). The age calibration and the construction of an age–depth model was performed with the Bacon program (Blaauw and Christen, 2011). The Bacon program performs a Bayesian age–depth modeling that includes the dating probability distribution and excludes negative sedimentation rates.

3.2. Geochemical analyses

The bulk geochemical sediment composition was acquired non-destructively at the core surface using the Avaatech X-Ray Fluorescence (XRF) core scanner at NIOZ (Texel, the Netherlands; Richter et al., 2006). XRF scanning was performed every 0.5 cm after the core surface was carefully cleaned and covered with a SPEXCerti Ultralene foil (Tjallingii et al., 2007). Analyses were performed at 10 kV for 10 s, and at 30 kV for 20 s in combination with a Pd-tick filter. These two settings provided analyses of 13 elements (Al, Br, Ca, Cl, Fe, K, Mn, Rb, S, Si, Ti, Zn and Zr). Biplot

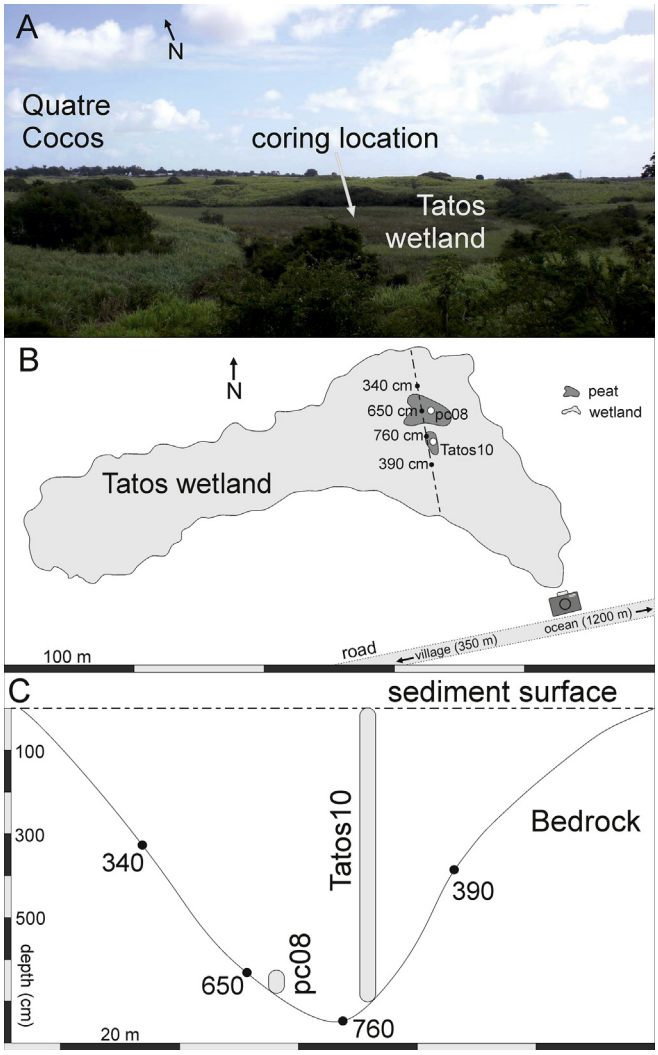

Fig. 2. Photograph and schematic representation of Tatos wetland. Figure A shows the coring location and the village Quatre Cocos (photo courtesy by EJdB). Figure B shows the location of the coring sites and measured sediment thickness. Tatos10 is the core analyzed in this study; pc08 is a shorter parallel core taken in 2008. Figure C shows a schematic cross section through the basin showing the bathymetry along the dotted line indicated in B.

diagrams of the first two principal components (PCs) were used to visualize the compositional differences. Accordingly, elements that reveal the main compositional variations were selected as ratio pairs of element intensities. Element intensities are presented as log ratios that are normally distributed and linearly related to log ratios of element concentration (Weltje and Tjallingii, 2008).

For ostracod analysis moist samples (n = 80) weighing ~4 g were taken every ~10 cm along the core and put into conical jars filled with deionized water and placed on a 63 μm mesh and oven dried at 40 °C. The coarse fraction was observed under a stereomicroscope. Between 10 and 15 adult valves of *Cyprideis torosa* were handpicked from each sample. *C. torosa* valves were chosen as they were abundant throughout the sequence and can live in a wide range of salinities varying from 0.5 to 60‰ (De Deckker, 1981). Juveniles were excluded and either left or right valves were selected to reduce the possible influence of vital effects (Heaton et al., 1995). Each valve was cleaned with a brush and distilled water under a binocular microscope.

Stable isotope analysis was carried out on 10 to 15 adult valves of *Cyprideis torosa*. The ostracods were treated with 100% orthophosphoric acid at 25 °C and analyzed on a gas bench in the Department of Earth Science, University of Cambridge. The analytical precision was 0.1‰. Additional samples (n = 22) for isotope analysis were taken between 180 and 340 cm on bulk $CaCO_3$ at additional depths. Stable isotope results ($\delta^{13}C$ and $\delta^{18}O$) are reported in the standard delta (δ) notation in parts per mil (‰) relative to the international VPDB standard.

3.3. Analyses of pollen and diatoms

The Tatos core was sampled every 20 cm for pollen and diatom analyses by extracting 1 cm thick slices. Additionally, intervals of particular interest were sampled every 10 cm. Diagrams were plotted with TILIA 1.5.12 (Grimm, 1993, 2004) software. Zonation was determined by CONISS analysis, included in the TILIA program.

Pollen samples (n = 35) were prepared using standard pretreatment techniques including sodium pyrophosphate, acetolysis and heavy liquid separation with a bromoform–ethanol mixture, specific gravity 2 (Faegri and Iversen, 1989). Additional details on sample preparation and pollen identification are described in Van der Plas et al. (2012). Pollen identifications in this study were predominantly based on modern pollen samples collected by De Boer, Baider and Florens. Microscopic charcoal was classified into size classes 30–60 μm, 60–200 μm, and >200 μm.

Approximately 0.8 cm^3 of each sample (n = 79) was prepared for diatom analysis. Samples were immersed in 30 ml of H_2O_2 (30%) for 30 min at room temperature, after which few drops of potassium permanganate were added. After the reaction stopped, 10 ml of HCl was added. Samples were then washed with distilled water, mounted in naphrax on permanent slides and analyzed with an Olympus microscope at ×1000 magnification. A minimum of 400 valves was counted per sample. Diatom taxonomy and ecology were identified after Evans (1958), Gaiser and Johansen (2000), Krammer and Lange-Bertalot (1999), Patrick and Reimer (1966), Sala et al. (2002), Gasse (1986) and Witkowski et al. (2000).

3.4. Hydrogeological analyses

The influence of periods of enhanced seasonal precipitation and short-term tidal variations on the subsurface fresh- to salt-water boundary was recorded in Tatos between August 2010 and August 2011 at 1-h intervals using data-logging pressure transducers (Schlumberger Water Service Divers®). The electrical conductivity (EC) of the surface water in Tatos was measured during the field season in August 2010.

4. Results

4.1. Chronology

The radiocarbon chronology of the sediment core is based on 16 carefully selected macro-organic samples (Table 1). Seeds and plant remains originate from vegetation in the direct vicinity of the basin and have not been transported or reworked. The sample at 424 cm contained insufficient carbon for a reliable radiocarbon analysis. A reversed sample point at 202 cm was excluded for age-scale construction. The fourteen remaining ages reveal a continuous sedimentation from ~7967 cal yr BP to the present (Fig. 3). Sedimentation rates remain relatively constant between 735 and 226 cm, but decrease from 226 cm to the top.

Seven periods (TAT-1 to TAT-7) were identified based on lithology, XRF geochemistry and pollen and diatom zone transitions (Fig. 4). Period TAT-1 (735–540 cm; 7970–6820 cal yr BP) consists

Table 1
List of radiocarbon dates and sample-specific data.

Depth (cm)	Material	Lab. Number	^{14}C yr BP	Sigma	δ^{13}C	cal yr BP (1σ)	Rel ar u prob distr	cal yr BP (2σ)	Rel area u prob distr
66.5	Seeds	GrA-51609	260	±30	−19.83	154–170	0.257	148–220	0.527
						180–187	0.069		
						195–205	0.112	269–321	0.473
						278–307	0.562		
180.5	Seeds	GrA-51610	2450	±30	−25.59	2351–2460	1.000	2341–2500	0.867
								2596–2613	0.023
								2638–2692	0.109
202	Seeds	GrA-53326	4470	±35	−26.88	4878–4942	0.353	4863–5070	0.810
						4951–5046	0.638	5108–5125	0.019
						5209–5210	0.009	5168–5174	0.007
								5177–5276	0.164
226.5	Seeds	GrA-51611	3750	±35		3974–4090	0.984	3909–4103	0.889
						4133–4136	0.016	4107–4149	0.111
252	Macrofossils	GrA-53327	3885	±35	−27.84	4151–4294	0.974	4095–4121	0.052
						4334–4339	0.026	4145–4360	0.859
								4365–4408	0.088
268	Seeds	GrA-53328	3930	±35	−28.1	4244–4305	0.430	4157–4205	0.106
						4310–4318	0.051		
						4322–4357	0.252	4223–4417	0.894
						4367–4405	0.266		
285.5	Seeds	GrA-51612	4135	±35	−27.36	4448–4468	0.106	4437–4655	0.756
						4517–4625	0.740	4667–4707	0.075
						4763–4788	0.154	4756–4811	0.168
294.5	Seeds	GrA-51614	4125	±35	−30	4445–4474	0.179	4428–4649	0.812
						4479–4480	0.009	4671–4700	0.048
						4514–4616	0.699	4759–4807	0.139
						4765–4784	0.114	4834–4977	0.959
320	Seeds	GrA-51616	4385	±35	−28.57	4846–4891	0.572	5013–5033	0.041
						4899–4909	0.094		
						4926–4959	0.334		
424	Macrofossils	–	Failed	–	–	–	–	–	–
507	Seeds	GrA-51617	5810	±35	−26.9	6496–6568	0.654	6449–6655	1.000
						6585–6629	0.346		
567.5	Wood	GrA-51619	6195	±40	−30.61	6952–7029	0.507	6906–7163	1.000
						7044–7069	0.145		
						7078–7086	0.044		
						7111–7156	0.304		
591.5	Wood	GrA-51620	6395	±40	−27.39	7177–7211	0.212	7167–7333	0.885
						7243–7319	0.788	7354–7377	0.046
								7385–7415	0.069
653	Seeds	GrA-51621	6660	±40	−32.59	7440–7448	0.078	7432–7568	1.000
						7459–7514	0.658		
						7539–7561	0.264		
696	Seeds	GrA-51623	6910	±40	−29.01	7622–7648	0.191	7595–7601	0.009
						7650–7725	0.809	7606–7789	0.991
730	Seeds	GrA-51624	7045	±40	−26.9	7760–7774	0.085	7707–7883	0.804
						7784–7867	0.719	7886–7933	0.196
						7898–7924	0.196		

of peat with plant remains, large wood fragments, seeds of palm, *Ficus* and *Pandanus* and other macrofossils. Macrofossils disappear and organic matter content decreases after 570 cm (7060 cal yr BP). Siliciclastic sediment becomes abundant in periods TAT-2 to TAT-6 (540 and 68 cm; 6820–400 cal yr BP). Period TAT-7 (68–1 cm; 400 cal yr BP – present) is a peat layer that lies on top of the siliciclastic interval.

4.2. Geochemistry

The maximum variation in the XRF data is indicated by the PC 1 – PC 2 scatter plot (Fig. S1). The XRF data of the siliciclastic sediments show a strong negative correlation between the elements Ca, Sr and Br with the elements Ti and Fe. The element Ca is associated with biogenically produced calcium carbonate ($CaCO_3$), whereas the immobile element Ti is indicative of detrital sediments. Therefore, relative variations of biogenic $CaCO_3$ vs detrital input can be indicated with ln(Ca/Ti) values. High concentrations of Br in marine organic matter indicate that sedimentary Br can be used to trace marine versus terrestrial organic carbon (Mayer et al., 2007; Ziegler et al., 2008). Br concentration will increase when saline groundwater infiltrates at the Tatos basin and the production of organic matter in the basin shifts from terrestrial to marine. Accordingly, relative saline water influence at the Tatos basin can be indicated by ln(Br/Ti) values.

The gradual change from peat towards predominantly siliciclastic sediments after 570 cm (7060 cal yr BP) is indicated by increasing ln(Ca/Ti) values (Fig. 5). These values increase until 340 cm (5100 cal yr BP), interrupted by abrupt negative anomalies. After 340 cm ln(Ca/Ti) values drop and remain low until 188 cm (2700 cal yr BP), except around 295 cm (4650 cal yr BP). An increase of ln(Ca/Ti) is observed from 188 to 140 cm (2700–1700 cal yr BP), after which values decline. Several short and abrupt episodes are observed with low or high ln(Ca/Ti) values between 185 and 100 cm (2600–1000 cal yr BP) (Fig. 5). Values of ln(Br/Ti) are stable in the lowest part of the core until 540 cm. Subsequently, ln(Br/Ti) values exhibit a saw tooth pattern until 340 cm. Values drop after 340 cm and remain relatively stable until 90 cm (800 cal yr BP). High values of ln(Br/Ti) are recorded during the last 400 years, corresponding with the organic-rich top of the core.

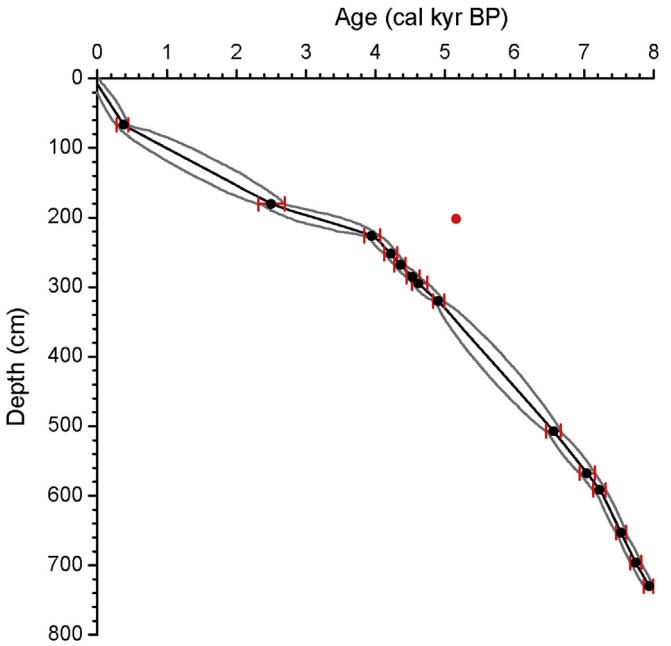

Fig. 3. Age model of the Tatos10 sediment core. Black dots represent radiocarbon dates, red lines indicate 2σ age distribution. Black line indicates 'best' age–depth model based on weighted mean from age distributions and gray lines indicate the chronological uncertainty (95%). The red dot indicates the date not used for age-model calibration. (For interpretation of the references to colour in this figure legend, the reader is referred to the web version of this article.)

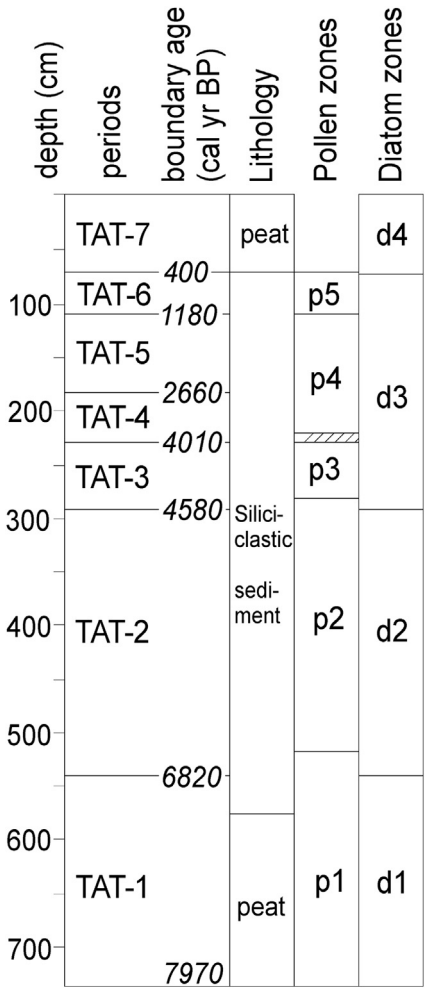

Fig. 4. Periods TAT-1 to TAT-7 and boundary ages from the Tatos core against depth, derived from transitions in the lithology and changes in downcore pollen and diatom assemblages.

The ostracod assemblage is monospecific, consisting entirely of the holeuryhaline species *Cyprideis torosa*. Monospecific assemblages are common in brackish water environments (Frenzel and Boomer, 2005). Adult ostracods were present in all samples between 535 and 75 cm, although in varying abundances. Ostracod valves were not present above and below these levels. The $\delta^{18}O$ of *C. torosa* ranges between −2.56‰ and 2.22‰, whilst the $\delta^{13}C$ ranges between −8.17‰ and −0.46‰ (Fig. 5). The $\delta^{13}C$ and $\delta^{18}O$ values of the additional bulk $CaCO_3$ samples fit well with the ostracod samples, although $\delta^{13}C$ values tend to be higher in the bulk $CaCO_3$ samples. From 535 to 515 cm (6780–6630 cal yr BP), $\delta^{18}O$ and $\delta^{13}C$ values are generally more negative. From 505 cm (6540 cal yr BP) there is a shift to more positive $\delta^{18}O$ values, which continues for the remainder of the ostracod sequence. ^{18}O-depleted phases occur around 6300, 5450, 5150, 4750, 4350 and 4150 cal yr BP superimposed on the generally more positive $\delta^{18}O$ trend (Fig. 5). The $\delta^{13}C$ sequence is generally more positive from 490 to 280 cm (6410–4480 cal yr BP) and 185 to 75 cm (2630–520 cal yr BP), and generally more negative between 280 and 195 cm (4480 and 2950 cal yr BP) (Fig. 5). Both $\delta^{18}O$ and $\delta^{13}C$ exhibit a saw tooth pattern, with rapid fluctuations between 535 and 225 cm (6820–3920 cal yr BP). From 225 to 75 cm (3920–520 cal yr BP), there are fewer fluctuations in the $\delta^{18}O$ and $\delta^{13}C$ sequences.

4.3. Pollen and diatom analyses

Pollen preservation varied from good to poor throughout the sediment core; samples between 65 and 5 cm did not contain enough pollen grains to acquire a meaningful pollen spectrum. CONISS identified zone boundaries at 515 (6630 cal yr BP), 290 (4580 cal yr BP) and 110 cm (1180 cal yr BP) and an outlying pollen spectrum at 225 cm (3930 cal yr BP). A concise description of the pollen zones is provided in Table S1. Pollen taxa reflect palm woodland, semi-dry lowland forest and wetland vegetation (Fig. 6A). Palm woodland is mainly represented by *Latania*, *Dictyosperma* and *Pandanus*. Species of *Pandanus* can be found from wet environments to dry coastal regions (Vaughan and Wiehe, 1937). However, the concurrence of *Latania* and *Dictyosperma* suggests that our record predominantly reflects *Pandanus vandermeeschii*, a common species in palm woodland (Vaughan and Wiehe, 1937; North and Bullock, 1986). Semi-dry forest is characterized by trees of *Ficus*, *Eugenia* spp., *Sideroxylon* spp., *Molinaea*, *Diospyros* spp., *Protium obtusifolium*, cf. *Premna*, *Foetidia*, *Terminalia bentzoë*, *Tabernaemontana* and shrubs of *Dodonaea* and *Dombeya*. Species of palm woodland are predominantly found in environments with an MAP of <1000 mm; semi-dry forest species are predominantly found in environments with MAP of 1000–1500 mm. Palm woodland of the driest areas of Mauritius are characterized by *Latania*, whereas *Eugenia* trees are most common for the more humid semi-dry forest. Both species are significantly present throughout the core, except for the lowest and highest pollen sample. Therefore, log ratios of *Latania* and *Eugenia* pollen counts were used to infer climate conditions from the vegetation reconstruction (Fig. 6A).

The diatom record shows four zones with boundaries at 540 (6820 cal yr BP), 290 (4580 cal yr BP) and 70 cm (420 cal yr BP) (Fig. 6B). The record consists mainly of brackish, alkaliphilous and

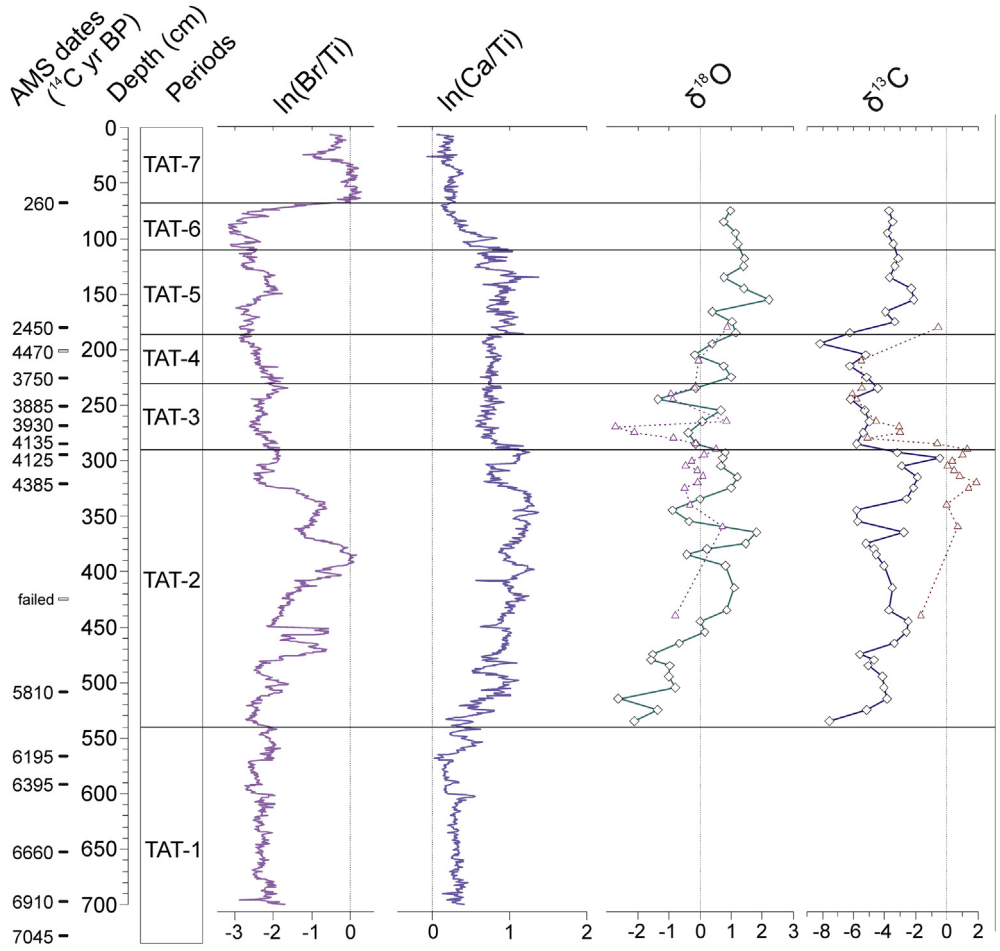

Fig. 5. Records of geochemical elements and isotopes. From left to right are shown: ^{14}C dates (open rectangles were not used for the age-model calibration), periods, ratios of ln(Br/Ti) and ln(Ca/Ti), and stable isotopes $\delta^{18}O$ and $\delta^{13}C$. Diamonds indicate ostracod samples and triangles indicate bulk $CaCO_3$ samples.

freshwater but saline tolerant diatoms, but alternate with peak occurrences of saline and freshwater diatoms. A concise description of the diatom zones is provided in Table S2.

4.4. Hydrology

Water level fluctuations for periods of 1 year (Fig. 7a) and 15 days (Fig. 7b) in the Tatos basin and lake Planche, a small lake at ~0.75 km distance from Tatos and ~1.0 km from the ocean, show tidal fluctuations of respectively ~2 and ~3 cm. The effect of ocean spring tides (about twice a month) is distinct in lake Planche but not in Tatos. Both tidal records show that water level changes in the basins are driven by changing ocean levels and rainfall events. Water level rises more than would be expected from local precipitation; we relate this offset to inflow of groundwater from the surrounding higher grounds. A decrease in water level, for example during the months of April to July, is caused by the combined effect of evapotranspiration and subsurface outflow towards the ocean. Planche showed a much faster water level decrease after a rainfall event indicating a much faster subsurface drainage towards the ocean. Conductivity measured on surface water of Tatos had an EC value of 2.8 mS/cm reflecting slightly brackish conditions. Conductivity of Planche water was higher with an EC of 6.0 mS/cm. The data show that both wetlands are overlying a salt water wedge formed by sea water intrusion, a common setting in coastal areas (e.g. Oude Essink, 1996).

Meteorological variations may have an effect on the water salinity in Tatos in two different ways. First, the water level and salinity in the basin are controlled by precipitation and the inflow of fresh groundwater from the surrounding area and evapotranspiration. Increased precipitation and inflow of fresh groundwater will increase the level of fresh groundwater and water table in the Tatos basin. Second, increased discharge of fresh groundwater in the area around the Tatos basin will prevent the intrusion of the salt groundwater. Low surface water levels in the basin and groundwater levels in the surroundings will enhance the supply of saline groundwater in the basin.

5. Environmental reconstruction and discussion

5.1. Holocene environmental and depositional history of Tatos

Coral growth reconstruction indicated that the sea-level at Mauritius rose at a relatively constant rate between ~8000 and ~2500 cal yr BP from approximately 8 m below present sea level to the current sea level high stand (Camoin et al., 2004). The rising sea level caused an inland migration of the coastline and rising groundwater table of the coastal lowlands. Eventually the groundwater table progressively inundated the Tatos basin and initiated wetland vegetation in this relatively dry region (Fig. 8A). Sediment started to accumulate after 8000 cal yr BP indicating that the Tatos depression was filled with water. Present-day relative groundwater levels increase due to tidal fluctuations and rainfall,

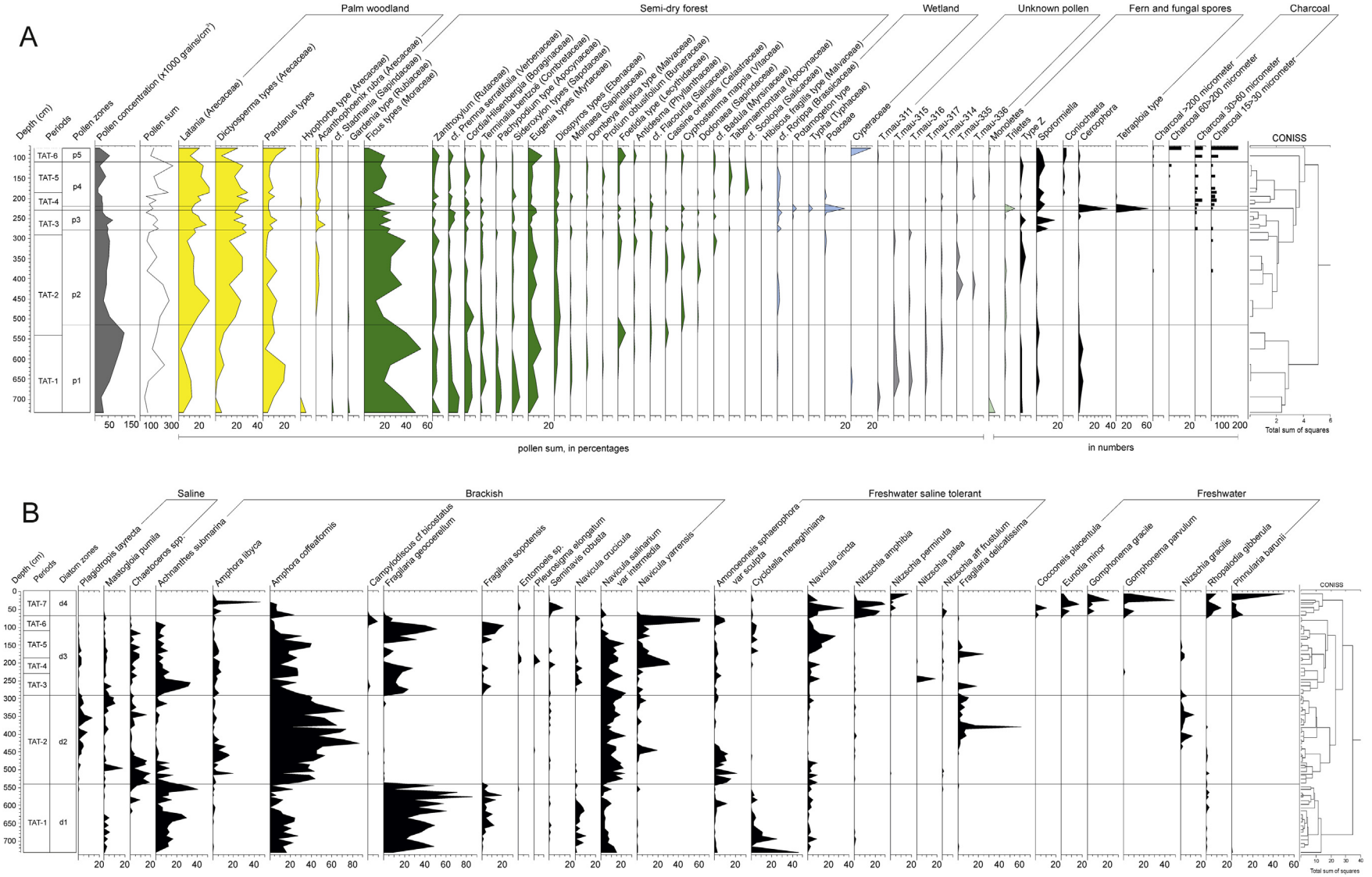

Fig. 6. Pollen and diatom records from the Tatos core. Figure A shows pollen zones, pollen concentration record and pollen sum values, records of individual pollen taxa, fern taxa and fungal spores, charcoal record and CONISS cluster diagram. Figure B shows diatom zones, records of individual diatom taxa and the CONISS cluster diagram. Pollen and diatom taxa with less than two occurrences are not shown.

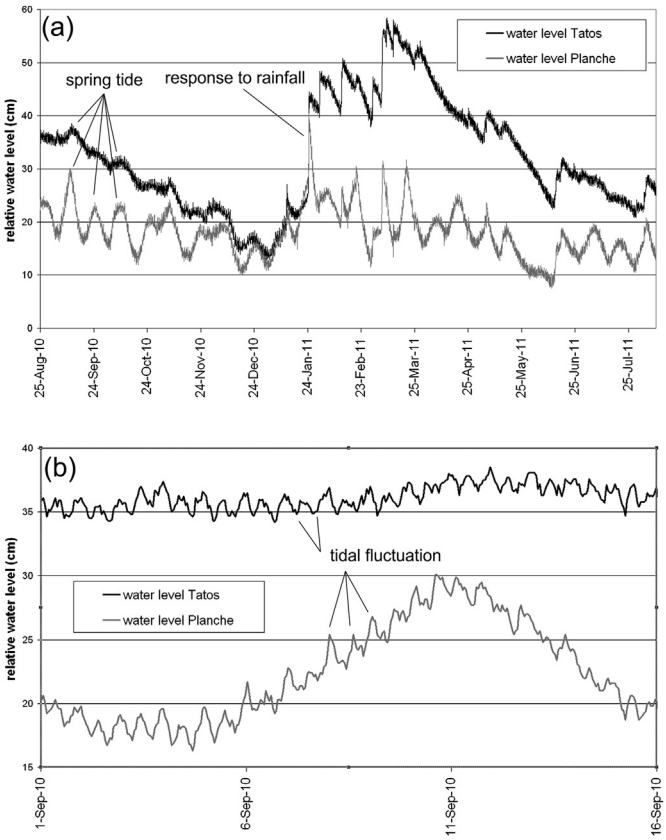

Fig. 7. Water level fluctuations measured in Tatos and Planche showing responses to sea level changes and rainfall event for periods of (a) 1 year and (b) 15 days.

when groundwater discharge from higher ground increases (Fig. 7). Vertical variations of the ground-water levels also vary the interface between fresh and salt groundwater, and consequently the water in the Tatos depression.

5.1.1. Period TAT-1: 7970–6820 cal yr BP, 736–540 cm

The peat layer at the bottom part of the core covers the period from 7970 to 7060 cal yr BP and contains brackish and saline-tolerant freshwater diatom species. This indicates that the Tatos basin was influenced by both the inflow of fresh groundwater as well as brackish-saline groundwater. Frequent changes in the diatom species composition suggest repeated salinity changes that result from variations of the interface between fresh and salt groundwater. These salinity changes are not evidently indicated by the ln(Br/Ti) values, which is probably due to the lack of marine organic matter.

Seeds, wood fragments and other macrofossils in combination with spores of coprophilous fungi indicate the presence of vegetation growing in the basin (Fig. 8A). This vegetation suggests standing freshwater in the basin and that attracted giant tortoises (*Cylandraspis* sp.) and dodos (*Raphus cucullatus*). Macrofossils, and thus local vegetation, abruptly disappear around 7060 cal yr BP followed by an increase of siliciclastic sediment. Regional sea-level reconstructions show a slight acceleration between 7500 and 7000 cal yr BP (Camoin et al., 2004). Permanent wet and probably brackish conditions in the basin drowned local vegetation due to the rising groundwater level after 7060 cal yr BP. The pollen record shows abundant *Ficus*, *Eugenia*, *Sideroxylon* and *Diospyros* as well as *Pandanus*, which indicate semi-dry forest and palm wood in the eastern coastal lowlands. The presence of palm woodland and semi-dry forest, and low ln(*Latania*/*Eugenia*) ratios between 7970 and 6820 cal yr BP suggest similar climatic conditions to the present-day (Fig. 9).

5.1.2. Period TAT-2: 6820–4580 cal yr BP, 540–290 cm

Sedimentation changed from organic rich-clay to laminated clay around 6820 cal yr BP, which corresponds to the first appearance of ostracods and the transition from a predominant abundance of benthic to planktonic diatoms. These changes indicate that the swamp environment changed into a shallow lake with frequently changing fresh, brackish, and saline waters (Fig. 8B). Frequent variations in salinity is indicated by the diatom species and strong variations in the ln(Br/Ti) record. Increasing ln(Ca/Ti) and ln(Br/Ti) values after 6820 cal yr BP indicate an increasing production of biogenic carbonate and marine organic matter due to more saline conditions. Enhanced saline water infiltration is also reflected by the disappearance of low salinity diatom species *Fragilaria geocoerellum*, which are replaced by the saline species *Amphora coffeaformis* and *Chaetoceros* spp. In particular *A. coffeaformis* require environments with high magnesium and calcium concentrations for its motility (Sylvestre et al., 2001), which are common in sea water.

The shift towards less depleted $\delta^{18}O$ and $\delta^{13}C$ values as well as increasing proportions of palm woodland pollen and of ln(*Latania*/*Eugenia*) values indicate increasing aridity after 6820 cal yr BP (Fig. 9). The pollen data indicate peak values around 6100 cal yr BP suggesting that generally drier conditions established around this time and remained until 4580 cal yr BP.

The ln(Ca/Ti) and ln(Br/Ti) show several abrupt changes between 6820 and 4580 cal yr BP, which are similar but not identical (Fig. 9). The abrupt changes to high ln(Ca/Ti) values reveal periods

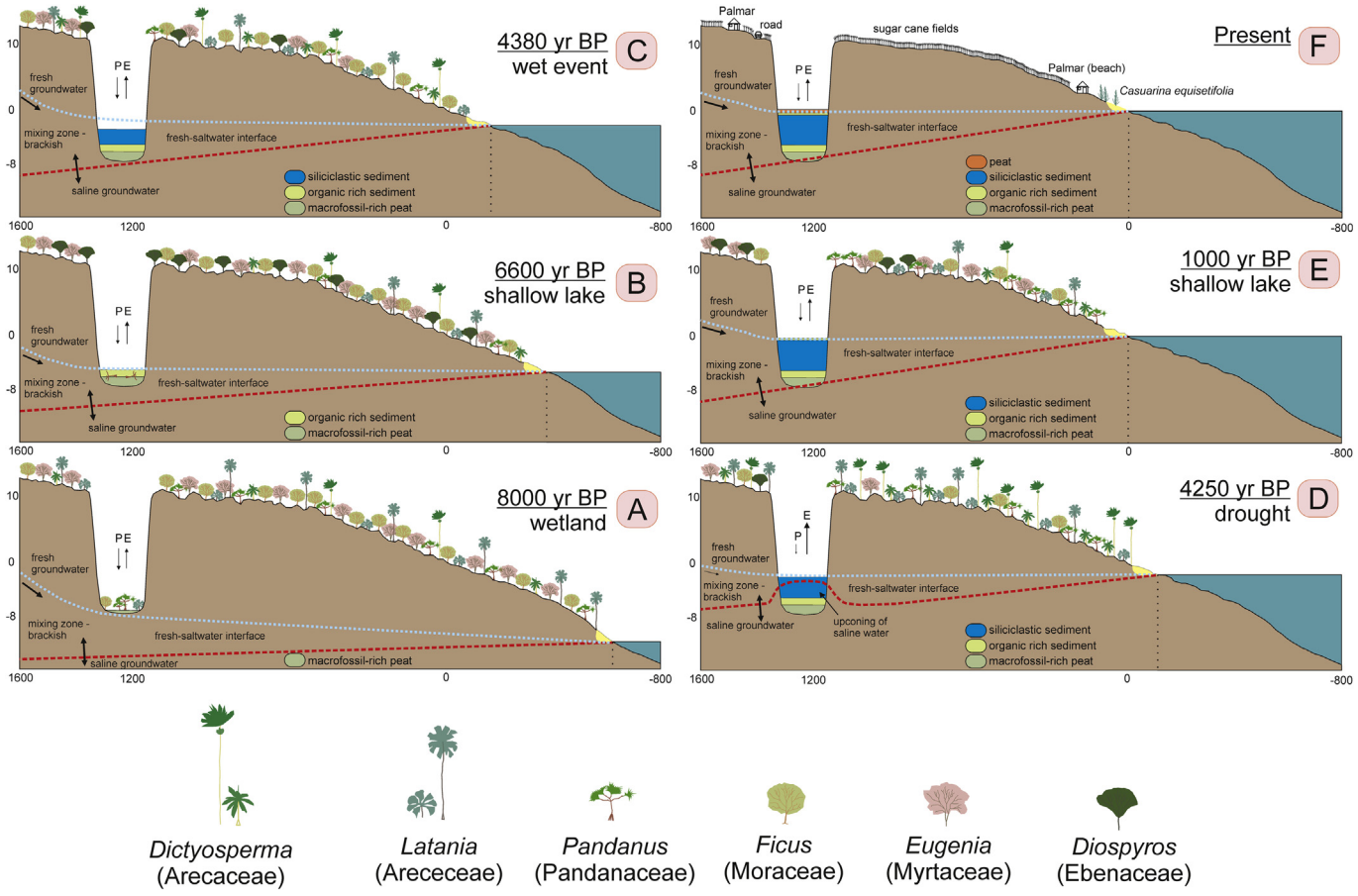

Fig. 8. Schematic environmental reconstruction of the Tatos basin in relation to the changing coastline and the surrounding coastal lowlands at different times (A–F). The accumulation of sediment in the Tatos basin is driven by sea level rise. Wet events (C) and droughts (D), indicated by changing precipitation and evapotranspiration arrows, mark changes in the hydrology of the basin caused by shifting boundaries of saline and fresh groundwater. Trends of vegetation change are shown by six main plant species *Pandanus*, *Dictyosperma* and *Latania* (palm woodland), *Eugenia* and *Diospyros* (semi-dry evergreen forest) and *Ficus* (palm woodland and semi-dry evergreen forest).

with relatively high carbonate production and less siliciclastic sediments, whereas abruptly increasing ln(Br/Ti) values indicate a relative increase of marine organic matter. Most likely, the production of biogenic carbonate and marine organic matter do not respond identically to salinity changes, which explains most of the differences between the records of ln(Ca/Ti) and ln(Br/Ti). Nevertheless, these records are interpreted by changes of the interface between fresh and saline groundwater, where high values are associated to periods of increased saline water infiltration during generally dry conditions. Alternatively, high ln(Ca/Ti) values could also result from increased aeolian transport of detrital $CaCO_3$ from carbonate-rich beach deposits, which might explain the relatively large difference between ln(Ca/Ti) and ln(Br/Ti) around 4650 cal yr BP. Periods with increased freshwater but saline tolerant diatom species, reduced ln(Ca/Ti) values and depleted $\delta^{18}O$ and $\delta^{13}C$ values occur at 6650, 6300, 6050, 5700, 5500, 5150 and 4750 cal yr BP, reflecting events of increased rainfall and freshwater runoff in a generally more arid landscape and waters of higher salinity (Fig. 9).

5.1.3. Period TAT-3: 4580–4010 cal yr BP, 290–230 cm

The siliciclastic sediments deposited between 4580 and 4010 cal yr BP reveal elevated proportions of palm woodland, brackish diatoms and depleted isotopic values suggesting consistently arid conditions (Fig. 9). The driest conditions during this highly variable period are recorded between 4350 and 4180 cal yr BP, inferred from the maximum recorded extent of palm woodland and high values of ln(*Latania*/*Eugenia*), peak values of brackish and marine diatoms, and increased values of $\delta^{13}C$ and $\delta^{18}O$ (Fig. 8D). Consistently low ln(Ca/Ti) and ln(Br/Ti) values suggest that the production of carbonate and marine organic matter was minimal. Peak values of freshwater diatoms match strong negative excursions of $\delta^{18}O$ values around 4380 and 4150 cal yr BP. These two incursions of increased freshwater groundwater discharge are interpreted as distinct wet events (Fig. 8C), similar as the repeated wet events between 6650 and 4750 cal yr BP.

5.1.4. Period TAT-4: 4010–2660 cal yr BP, 230–186 cm

The siliciclastic sediments covering this period contain predominantly brackish and freshwater but saline tolerant diatoms, and the lowest proportion of saline diatoms compared to earlier periods. Additionally, the presence of saline diatom resting spores indicates unfavorable conditions for saline diatoms. The relatively stable isotopic values suggest prevailing lacustrine conditions without strong variations of the interface between fresh and saline groundwater. The return of coprophilous fungi suggests salinity had sufficiently reduced to make the water suitable for animals to drink (Fig. 5A).

An anomalous pollen sample at 3900 cal yr BP (225 cm) shows a rapid increase of Poaceae, charcoal and non pollen palynomorph (NPP) types. As most of these NPP types grow in soils, we suggest that grasses, charcoal and NPPs reflect erosion from sides of the basin. Erosion material could have been augmented by a dry event, such as the maximum dry conditions recorded at 4350–4180 cal yr

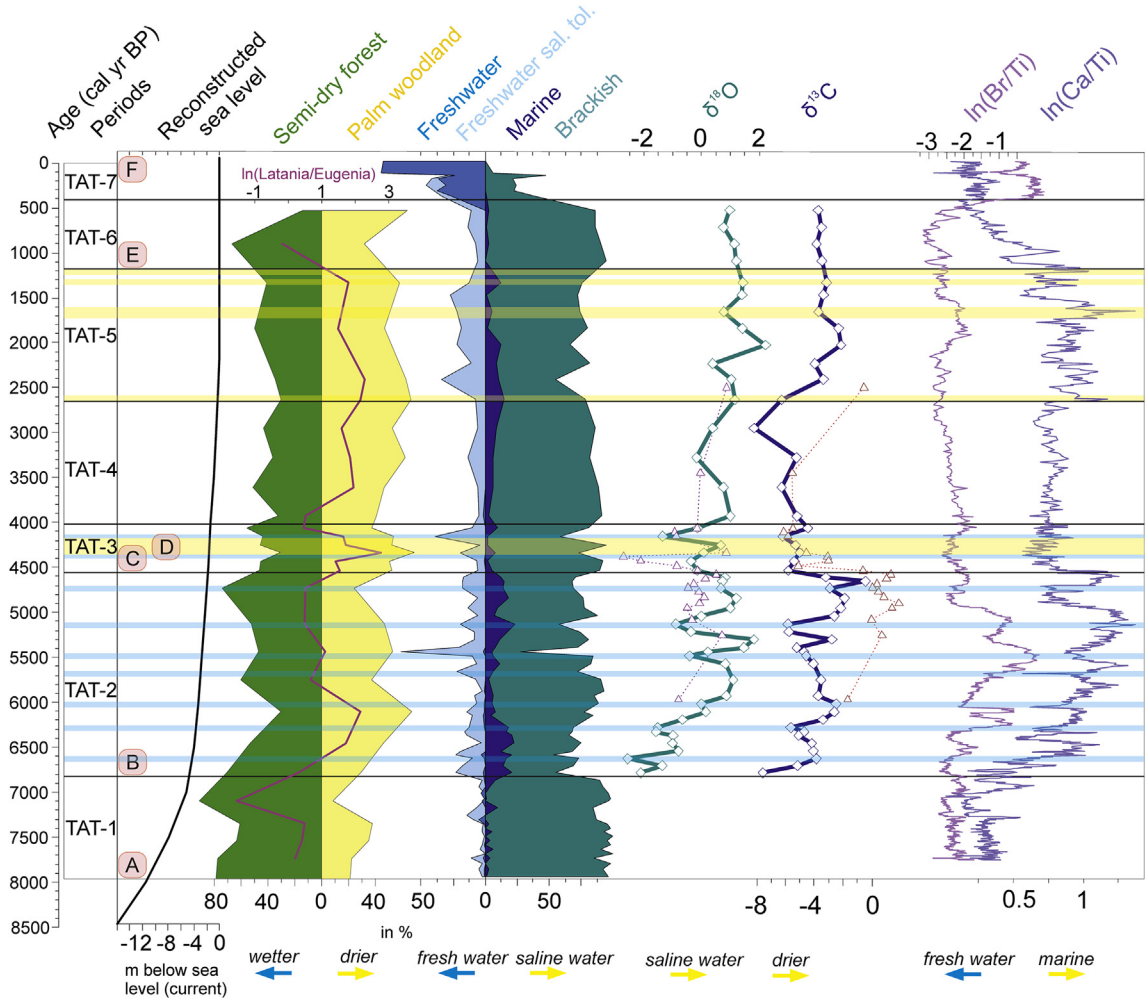

Fig. 9. Summary diagram showing various proxy records from the Tatos core against age. From left to right are shown: periods, sea level curve of the SW Indian Ocean (after Camoin et al., 2004), changing proportions of semi-dry forest and palm woodland, ln(*Latania*/*Eugenia*) ratios, diatom groups, stable isotopes from ostracods (diamonds and unbroken lines) and bulk $CaCO_3$ (triangles and dotted lines), and records of element ratios ln(Ca/Ti) and ln(Br/Ti). Letters A–F indicate snapshot reconstructions shown in Fig. 8.

BP. A decline in representation of both palms and trees (Fig. 9) suggests a reduction in vegetation cover following this drought. Opportunistic grasses and ferns became abundant and increase the potential risk for fire, explaining the high charcoal content in this interval.

Climatic conditions remained relative dry between 4010 and 2660 cal yr BP as suggested by high abundances of palm woodland, high values of ln(*Latania*/*Eugenia*) and the increasing amounts of microscopic charcoal suggesting frequent fire events (Fig. 9). A new fire regime and new forest elements *P. obtusifolium*, *Tabernaemontana* and cf. *Scolopia* might suggest a change in seasonality towards longer dry seasons (Marchant and Hooghiemstra, 2004) (Fig. 6A).

Reduced sedimentation rates and relatively low ln(Ca/Ti) and ln(Br/Ti) values between 4010 and 2660 cal yr BP suggest that the production of carbonate and marine organic matter remained low. Sediment transport to the lake was limited during dry climatic conditions and conditions for primary producers were probably unfavorable when water tables and groundwater levels were low.

5.1.5. Period TAT-5: 2660–1180 cal yr BP, 186–110 cm

The abundance of palm woodland remains stable and indicates persistently low humidity conditions. However, a shift towards higher ln(Ca/Ti) values, slightly less depleted stable isotopes and an increase in both saline and freshwater diatoms indicate an increase of climate variability after 2660 cal yr BP (Fig. 9). Coral reconstructions of past sea levels indicate that sea level reached its current position around 2500 cal yr BP. Consequently, Tatos would be more influenced by freshwater input as groundwater levels would no longer be driven by rising sea levels. However, stable sea levels would not explain the less depleted stable isotope values and increased ln(Ca/Ti) ratios. Peak values of ln(Ca/Ti) record higher input of biogenically produced $CaCO_3$ around 2600, 1350, 1200 and between 1700 and 1600 cal yr BP. These events of increased aeolian transport of $CaCO_3$, coinciding with less depleted stable isotope values, suggest periods of higher storm activity during droughts (Fig. 9).

5.1.6. Period TAT-6: 1180–400 cal yr BP, 110–68 cm

Brackish diatoms prevail, whereas the proportion of freshwater diatoms decline and saline species are nearly absent (Fig. 9). A shift from planktonic to benthic and epiphytic diatoms and relatively enriched $\delta^{13}C$ values suggests progressive sediment infilling of the shallow lake. Stable isotopic records remain at constant values and the disappearance of laminae within the siliciclastic sediments suggests stable water depth conditions and marginal marine influence. Increasing presence of fungi and phytoliths in the diatom

and pollen samples also indicate more terrestrial conditions. The decline of palm woodland vegetation and increase of semi-dry forest and low ln(*Latania*/*Eugenia*) values suggest wetter climate conditions (Fig. 8E).

5.1.7. Period TAT-7: 400 cal yr BP–present day, 68–1 cm

The upper 68 cm consists of well-mixed peat separated from the deposits below by a clear unconformity. Diatom compositions indicate that the Tatos wetland had progressed into a marshland with patches of peat during the last 400 years (Fig 8F), what coincides with human colonization of the island. Most likely, the Tatos depression was transformed from a lake to a bogland caused by sediment infilling and was possibly subject to reclamation for agriculture in a later stage. Human attempts for reclamation for agriculture by burning the original vegetation is further indicated by high charcoal content of the peat deposits between 65 and 45 cm depth.

The presence of palm woodland in the eastern lowlands throughout the middle and late Holocene is in contrast with the description of Cheke and Hume (2008), who suggested that palm woodland was restricted to the driest areas in the western coastal lowlands of Mauritius (Fig. 1). This contrast might be caused by increasing humid climate conditions of the last ~1200 years, during which semi-dry forest largely replaced the palm woodland and only persisted at the driest areas of Mauritius (De Boer et al., 2013a,b). However, the main cause would be the recent destruction of palm woodland by early colonizers, who used palms for consumption and construction material and cleared land for agricultural purposes (Cheke and Hume, 2008). Evidence for a strong impact of human activity in Mauritius is revealed by a drastic and rapid decline of palm taxa and palm-like growth forms (Cycadaceae, *Pandanus*, *Cyathea*) after colonization (De Boer et al., 2013a, b), including taxa extinction (Cycadaceae).

5.2. Holocene monsoon dynamics

Changing abundances of palm woodland and semi-dry forest, as well as ln(*Latania*/*Eugenia*) values were used to derive millennial-scale precipitation. Salinity and environmental reconstructions at Tatos based on diatoms, ostracods, stable isotopes, and sediment compositions showed numerous decadal and centennial droughts and wet events. To compare the inferred climate dynamics with other monsoon regions, we assume that monsoon precipitation in the SW Indian Ocean is determined by two moisture sources. As Mauritius receives most precipitation from the northeast monsoon during the austral summer, precipitation changes is partially driven by changes in southern hemisphere monsoon intensity. Furthermore, modern observations show that the southern equatorial Indian Ocean is the dominant source of moisture for the Asian boreal summer monsoons, indicating that Mauritius shares a common moisture source with ISM and ASM rainfall (Rohling et al., 2009; Clemens et al., 2010).

Increased low-latitude insolation during the early Holocene strengthened the monsoon systems and displaced the monsoon rainfall belt north of the equator northwards, strengthening the ISM (Gupta et al., 2005; Fleitmann et al., 2007) and ASM (Wang et al., 2005), and determined the African Humid Period (Blanchet et al., 2013). In contrast, dry conditions were recorded in the southern hemisphere monsoon regions such as the Australian-Indonesian summer monsoon (AISM; Griffiths et al., 2010).

In Mauritius, pollen records from the uplands record wettest vegetation types in the early Holocene (Van der Plas et al., 2012; De Boer et al., 2013b). The first period in the Tatos record also documents relatively humid conditions in the lowlands between 8000 and 6800 cal yr BP, corresponding to stronger northern hemisphere monsoon dynamics (Fig. 10). Humidity in Mauritius gradually decreased after 6800 cal yr BP as indicated by the expansion of palm woodland and less depleted isotope values. This coincides with the gradual decreasing strength of both ISM and ASM rainfall (Gupta et al., 2005; Wang et al., 2005; Fleitmann et al., 2007) (Fig. 10), due to the continuous southward migration of the mean boreal summer ITCZ. The decreasing trend in humidity in the Mauritian lowlands ceased after ~6000 cal yr BP, whilde relatively dry climate conditions persisted during the middle Holocene. Mauritian precipitation patterns are not completely similar with northern hemisphere summer monsoons and are therefore not solely driven by the precession-driven southward migration of the ITCZ.

A distinct contrast between western and eastern Indian Ocean climate is present throughout the middle Holocene, as AISM rainfall is enhanced between 7500 and 4000 cal yr BP (Denniston et al., 2013) (Fig. 10). Higher AISM rainfall corresponds to warmer waters in the Indonesian shelf (Stott et al., 2004) reflecting a warm Indo-Pacific Warm Pool (IPWP) (Abram et al., 2009). Despite overall higher precipitation if compared to the early Holocene, rainfall patterns throughout the Australian–Indonesian region were not uniform between ~7000 and ~4000 cal yr BP. Climate reconstructions from stalagmites in Borneo (Partin et al., 2007), Flores (Griffiths et al., 2009) and tropical western Australia (Denniston et al., 2013) reveal strong regional differences in the AISM intensity. These regional differences have been associated to meridional shifts in the austral summer ITCZ related to El Niño-Southern Oscillation (ENSO) dynamics (Denniston et al., 2013). However, an anti-phased relationship between Flores and Borneo has been related with a prolonged positive phase of the IOD. Positive IOD events are identified by cool and dry conditions in the eastern part of the Indian Ocean, and warm and humid conditions in the equatorial western Indian Ocean and East Africa (Saji et al., 1999; Marchant et al., 2006). A positive IOD-like configuration may be caused by strengthened ASM surface winds that enhanced upwelling in the eastern Indian Ocean, thereby producing a more easterly zonal wind component along the equator (Abram et al., 2007, 2009).

The Tatos records show reduced humidity in the SW Indian Ocean during the middle Holocene (Fig. 9). These relative dry conditions correspond with decreasing strength of ISM (Gupta et al., 2005) and decreasing ASM rainfall (Wang et al., 2005), higher AISM rainfall (Partin et al., 2007; Griffiths et al., 2010; Denniston et al., 2013) and distinct lower temperatures in the Kilimanjaro record between ~6500 and ~5000 cal yr BP (Thompson et al., 2002). These rainfall patterns demonstrate prolonged negative IOD-like configurations of the Indian Ocean during the middle Holocene (Fig. 10).

Superimposed on the generally dry climate conditions during the middle Holocene, the Tatos record identified multiple decadal to centennial wet events at ~6650, ~6300, ~6050, ~5700, ~5500, ~5150, ~4750, ~4380 and 4150 cal yr BP (Fig. 9). These events are indicated by peaks in freshwater diatoms, phases of depleted stable isotopes and rapidly shifting ln(Ca/Ti) values and are separated roughly every 350 years. The abrupt centennial-scale dry events associated with decreased strength of the IASM (Denniston et al., 2013) correspond to the middle Holocene wet events in Mauritius (Fig. 10). These events reflect positive IOD-like events, during which a northward shift of the ITCZ enhanced upwelling in the eastern Indian Ocean and strengthened ASM rainfall.

Driest conditions in the Mauritian lowlands are recorded between 4350 and 4180 cal yr BP, indicated by maximum extent of palm woodland and ln(*Latania*/*Eugenia*) values, high stable isotope ratios and peaks in marine diatom abundance (Fig. 9). An abrupt weakening of the northern hemisphere monsoons after 4400 cal yr

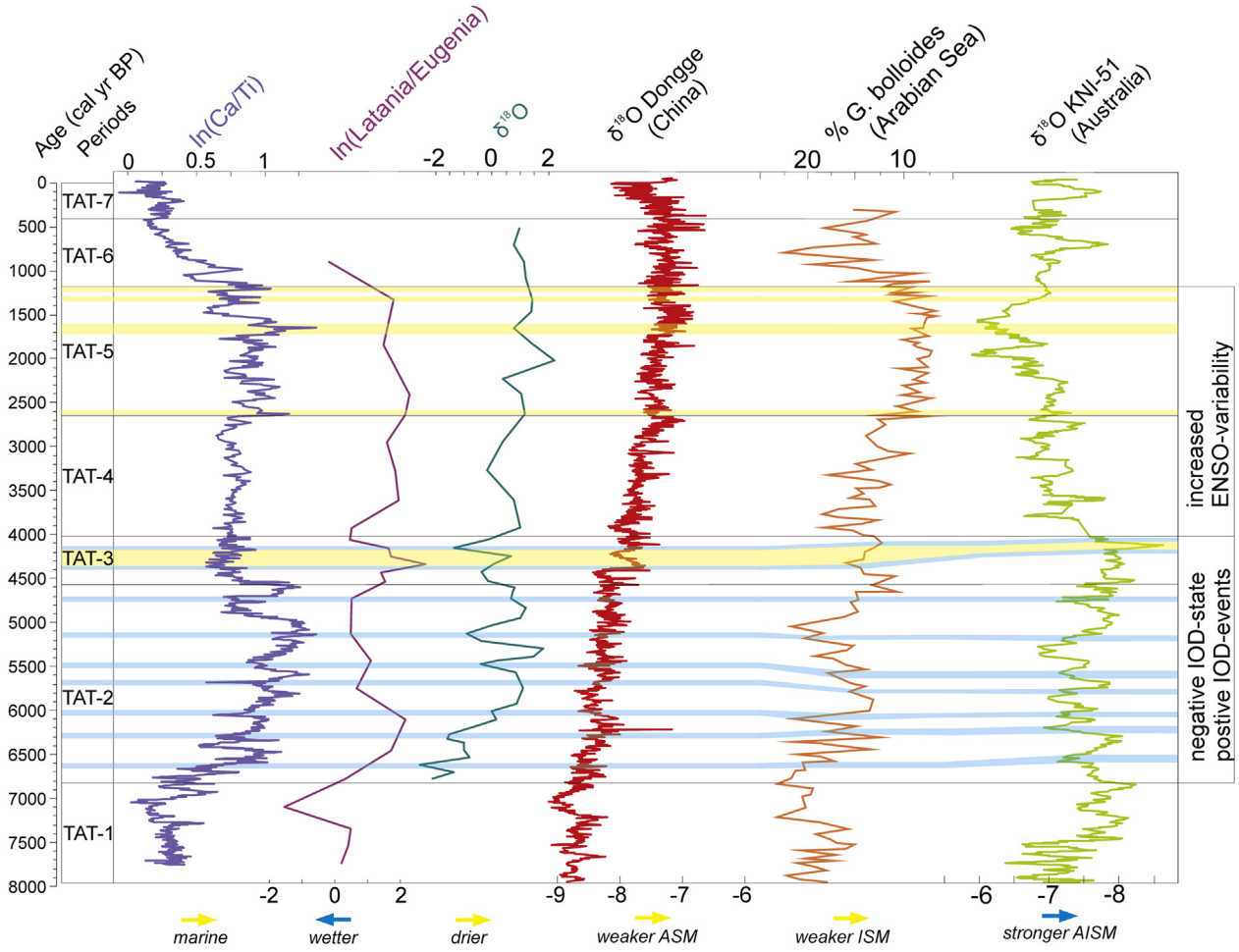

Fig. 10. Comparison of ln(Ca/Ti), ln(*Latania*/*Eugenia*) and $\delta^{18}O$ from ostracods from the Tatos core with monsoon records. Blue and yellow bars indicate wet events and droughts, respectively, inferred from the Tatos record, and show links with ASM rainfall from Dongge Cave, China (Wang et al., 2005), upwelling in the Arabian Sea (Gupta et al., 2005), and AISM rainfall from tropical western Australia (Denniston et al., 2013). (For interpretation of the references to colour in this figure legend, the reader is referred to the web version of this article.)

BP (Wang et al., 2005; Fleitmann et al., 2007) is considered as the initial cause of the collapse of a number of civilizations in Pakistan, India, Mesopotamia and eastern Africa (Cullen et al., 2000; Thompson et al., 2002; Staubwasser et al., 2003; Wang et al., 2005; MacDonald, 2011). This Holocene 'megadrought' coincides with dry conditions in the Mauritian lowlands, enhanced precipitation over the West Australian tropical regions (Denniston et al., 2013), and warm SSTs in the eastern equatorial Indian Ocean (Abram et al., 2009) (Fig. 10). Therefore, we suggest the 'megadrought' around 4300 cal yr BP represents an anomalously strong negative IOD event.

Climate conditions in the Mauritian lowlands were relatively stable between 4010 cal yr BP and 2660 cal yr BP, while humidity remained relatively low (Fig. 9). A rapid weakening of AISM rainfall is evident in western tropical Australia after 4200 cal yr BP (Denniston et al., 2013). Reduced precipitation in both the eastern and western equatorial Indian Ocean has been associated with weakening of AISM rainfall after 4200 cal yr BP (Partin et al., 2007; Griffiths et al., 2010; Denniston et al., 2013). Increased climate variations linked to ENSO-variability have been revealed in the Caribbean Sea (Donnely and Woodruff, 2007), Peru (Moy et al., 2002), the Eastern Pacific (Toth et al., 2012), the Galápagos islands (Conroy et al., 2008), the Indonesian shelf (Gagan et al., 2004) and Australia (Donders et al., 2008). These studies show that ENSO frequency and intensity increased between 5000 and 4000 cal yr BP and became the dominant forcing of late Holocene climate variability in tropical and subtropical regions (Moy et al., 2002; Gagan et al., 2004; Donders et al., 2007, 2008; Conroy et al., 2008; Toth et al., 2012).

Increasing input of biogenic $CaCO_3$ in the Tatos basin after 2660 cal yr BP reveals increased storm activity until ~1200 cal yr BP. Droughts and increased storm activity occur around 2600, 1650, 1300 and 1200 cal yr BP in the Mauritian lowlands (Fig. 9). These events correspond to weakening of the boreal summer monsoons (Wang et al., 2005; Fleitmann et al., 2007) and an abrupt reduction of upwelling in the Arabian Sea (Gupta et al., 2005) (Fig. 10). The Mauritian droughts and increased storm activity after 2660 are also linked with ENSO events in lake Pallcacocha in Peru at ~2600, ~1600 and ~1300 cal yr BP (Moy et al., 2002) and extreme ENSO events in the eastern Pacific at ~2500, ~2000 and ~1500 cal yr (Conroy et al., 2008; Toth et al., 2012), as well as lowest AISM rainfall between ~1500 and ~1200 cal yr BP in western tropical Australia (Denniston et al., 2013) (Fig. 10). Conroy et al. (2008) relate the shift at ~2600 cal yr BP to the decoupling of ENSO from the Atlantic ITCZ. Without the southward migrations of the Atlantic ITCZ into South America during which climate variability was

enhanced in the Cariaco Basin between ~4000 and ~2600 cal yr BP (Haug et al., 2001), ENSO events developed that also affected climate events in the SW Indian Ocean.

6. Conclusions

Mauritius experienced wet conditions between ~8000 and ~6800 cal yr BP, followed by decreasing humidity from 6800 to 6000 cal yr BP. Dry conditions persist until ~1200 cal yr BP, after which wetter conditions are recorded for the Mauritian lowlands and uplands (De Boer et al., 2013b). These climate changes correspond to northern hemisphere monsoon activity and suggest a link between Mauritian rainfall and ISM and ASM rainfall, as both receive moisture from the southern equatorial Indian Ocean.

The anti-phased relationship of climate dynamics between the Mauritian lowlands and western tropical Australia (Denniston et al., 2013) during the middle Holocene suggests a prolonged configuration of a negative IOD mode. A prolonged negative IOD-like state is supported by decreased ASM rainfall, higher AISM rainfall and lower temperatures in the Kilimanjaro record. Conversely, repeated decadal-scale wet events in the Mauritian lowlands occurring every ~350 years reflect short positive IOD-like events.

A shift in ENSO-activity around ~2600 cal yr BP signifies the decoupling of ENSO from the Atlantic ITCZ. Subsequently, ENSO affected the climate in the western Indian Ocean by increased storm activity and drought events after 2660 cal yr BP in Mauritius and reduced monsoon activity in the western and eastern Indian Ocean.

The onset of increased ENSO-activity after ~4000 cal yr BP was preceded by the driest conditions in the Mauritian lowlands recorded around 4300 cal yr BP. These driest conditions correspond to a global-scale period of monsoon weakening, which is considered as the driver of civilization collapses in Pakistan, Mesopotamia and eastern Africa (Cullen et al., 2000; Thompson et al., 2002; Staubwasser et al., 2003; Wang et al., 2005; MacDonald, 2011). This 'megadrought' coincides with wettest conditions in tropical western Australia (Denniston et al., 2013), and may therefore represent an anomalously strong negative IOD event.

Acknowledgments

We thank the Netherlands Organization for Scientific Research (project number ALW 819.01.009) for financial support. We thank Niels Hartog (Deltares, Utrecht) for valuable discussions on geochemical wetland processes and element compositions. We thank Annemarie Philip for preparing pollen and diatom samples. We appreciate the work and insight of Saskia Kroezen and Luc Chabanole. Maarten Blaauw (Queen's University, Belfast) is thanked for support to develop the age–depth model. The sugarcane company Omnicane (Mauritius) is greatly acknowledged for logistic support in the field.

Appendix A. Supplementary data

Supplementary data related to this article can be found at http://dx.doi.org/10.1016/j.quascirev.2013.12.026.

References

Abram, N.J., Gagan, M.K., Liu, Z., Hantoro, W.S., McCulloch, M.T., Suwargadi, B.W., 2007. Seasonal characteristics of the Indian Ocean Dipole during the Holocene epoch. Nature 445, 299–302.
Abram, N.J., McGregor, H.V., Gagan, M.K., Hantoro, W.S., Suwargadi, B.W., 2009. Oscillations in the southern extent of the Indo-Pacific Warm Pool during the mid-Holocene. Quat. Sci. Rev. 28, 2794–2803.
Berke, M.A., Johnson, T.C., Werne, J.P., Grice, K., Schouten, S., Sinninghe Damsté, J.S., 2012. Molecular records of climate variability and vegetation response since the Late Pleistocene in the Lake Victoria basin, East Africa. Quat. Sci. Rev. 55, 59–74.
Blaauw, M., Christen, J.A., 2011. Flexible paleoclimate age-depth models using an autoregressive gamma process. Bayesian Anal. 6, 457–474.
Blanchet, C.L., Tjallingii, R., Frank, M., Lorensen, J., Reitz, A., Brown, K., Feseker, T., Brückmann, W., 2013. High- and low-latitude forcing of the Nile River regime during the Holocene inferred from laminated sediments of the Nile deep-sea fan. Earth Planet. Sci. Lett. 364, 98–110.
Bosser, J., Cadet, T., Guého, J., Marais, W., 1976. Flore des Mascareignes – LaRéunion, Maurice, Rodrigues. MSIRI/ORSTOM-IRD/KEW, Port Louis, Mauritius.
Burney, D.A., Burney, L.P., Godfrey, L.R., Jungers, W.L., Goodman, S.M., Wright, H.T., Jull, A.J.T., 2004. A chronology for late prehistoric Madagascar. J. Hum. Evol. 47, 25–63.
Camoin, G.F., Montaggioni, L., Braithwaite, C., 2004. Late glacial to post glacial sea-levels in the Western Indian Ocean. Mar. Geol. 206, 119–146.
Castañeda, I.S., Werne, J.P., Johnson, T.C., Filley, T.R., 2009. Late Quaternary vegetation history of southeast Africa: the molecular isotopic record from Lake Malawi. Palaeogeogr. Palaeoclimatol. Palaeoecol. 275, 100–112.
Cheke, A., Hume, J., 2008. Lost Land of the Dodo: the Ecological History of Mauritius, Réunion, and Rodrigues. Poyser, London, UK, p. 480.
Clemens, S.C., Prell, W.L., 2007. The timing of orbital-scale Indian monsoon changes. Quat. Sci. Rev. 26, 275–278.
Clemens, S.C., Prell, W.L., Sun, Y., 2010. Orbital-scale timing and mechanisms driving Late Pleistocene Indo-Asian summer monsoons: reinterpreting cave speleothem $\delta^{18}O$. Paleoceanography 25, PA4207. http://dx.doi.org/10.1029/2010PA001926.
Conroy, J.L., Overpeck, J.T., Cole, J.E., Shanahan, T.M., Steinitz-Kannan, M., 2008. Holocene changes in eastern tropical Pacific climate inferred from a Galápagos lake sediment record. Quat. Sci. Rev. 27, 1166–1180.
Cullen, H.M., deMenocal, P.B., Hemming, S., Hemming, G., Brown, F.H., Guilderson, T., Sirocko, F., 2000. Climate change and the collapse of the Akkadian empire: evidence from the deep sea. Geology 28, 379–382.
De Boer, E.J., Hooghiemstra, H., Florens, F.B.V., Baider, C., Engels, S., Dakos, V., Blaauw, M., Bennett, K.D., 2013b. Rapid succession of plant associations on the small ocean island of Mauritius at the onset of the Holocene. Quat. Sci. Rev. 68, 114–125.
De Boer, E.J., Slaikovska, M., Hooghiemstra, H., Rijsdijk, K.F., Vélez, M.I., Prins, M., Baider, C., Florens, F.B.V., 2013a. Multi-proxy reconstruction of environmental dynamics and colonization impacts in the Mauritian uplands. Palaeogeogr. Palaeoclimatol. Palaeoecol. 383-384, 42–51.
De Deckker, P., 1981. Ostracods of athalassic saline lakes: a review. Hydrobiologia 81, 131–144.
Denniston, R.F., Wyrwoll, K.-H., Polyak, V.J., Brownd, J.R., Asmeromc, Y., Wanamaker Jr., A.D., LePointe, Z., Ellerbroek, R., Barthelmes, M., Cleary, D., Cugley, J., Woods, D., Humphreys, W.F., 2013. A stalagmite record of Holocene Indonesian-Australian summer monsoon variability from the Australian tropics. Quat. Sci. Rev. 78, 155–168.
Donders, T.H., Haberle, S.G., Hope, G., Wagner, F., Visscher, H., 2007. Pollen evidence for the transition of the Eastern Australian climate system from the post-glacial to the present-day ENSO mode. Quat. Sci. Rev. 26, 1621–1637.
Donders, T.H., Wagner-Cremer, F., Visscher, H., 2008. Integration of proxy data and model scenarios for the mid-Holocene onset of modern ENSO variability. Quat. Sci. Rev. 27, 571–579.
Donnely, J.P., Woodruff, J.D., 2007. Intense hurricane activity over the past 5,000 years controlled by El Niño and the West African monsoon. Nature 447, 465–468.
Evans, J., 1958. The survival of freshwater algae during dry periods. Part I. Ecology 46, 148–167.
Faegri, K., Iversen, J., 1989. Textbook of Pollen Analysis, fourth ed. Wiley, Chichester, UK.
Fleitmann, D., Burns, S.J., Mangini, A., Mudelsee, M., Kramers, J., Villa, I., Neff, U., Al-Subbary, A.A., Buettner, A., Hippler, D., Matter, A., 2007. Holocene ITCZ and Indian monsoon dynamics recorded in stalagmites from Oman and Yemen (Socotra). Quat. Sci. Rev. 26, 170–188.
Frenzel, P., Boomer, I., 2005. The use of ostracods from marginal marine, brackish waters as bioindicators of modern and Quaternary environmental change. Palaeogeogr. Palaeoclimatol. Palaeoecol. 225, 68–92.
Gagan, M.K., Hendy, E.J., Haberle, S.G., Hantoro, W.S., 2004. Post-glacial evolution of the Indo-Pacific Warm Pool and El Niño-Southern Oscillation. Quat. Int. 118–119, 127–143.
Gaiser, E., Johansen, J., 2000. Freshwater diatoms from Carolina Bays and other isolated wetlands on the Atlantic coastal plain of South Carolina, U.S.A., with descriptions of seven taxa new to science. Diatom Res. 15, 75–130.
Gasse, F., 1986. East African Diatoms – Taxonomy, Ecological Distributions. Bibliotheca Diatomologica, p. 201.
Gasse, F., Van Campo, E., 1998. A 40,000-yr pollen and diatom record from Lake Tritrivakely, Madagascar, in the southern tropics. Quat. Res. 49, 299–311.
Gasse, F., 2000. Hydrological changes in the African tropics since the Last Glacial Maximum. Quat. Sci. Rev. 19, 189–211.
Gordon, A.L., Ma, S., Olson, D.B., Hacker, P., Field, A., Talley, L.D., Wilson, D., Baringer, M., 1997. Advection and diffusion of Indonesian throughflow water within the Indian Ocean South Equatorial Current. Geophys. Res. Lett. 24, 2573–2576.
Griffiths, M.L., Drysdale, R.N., Gagan, M.K., Zhao, J.-X., Aylife, L.K., Hellstrom, J.C., Hantoro, W.S., Frisia, S., Feng, Y.-X., Cartwright, I., St. Pierre, E., Fischer, M.J.,

Suwargadi, B.W., 2009. Increasing Australian-Indonesian monsoon rainfall linked to early Holocene sea-level rise. Nat. Geosci. 2, 636–639.
Griffiths, M.L., Drysdale, R.N., Gagan, M.K., Frisia, S., Zhao, J.-X., Ayliffe, L.K., Hantoro, W.S., Hellstrom, J.C., Fischer, M.J., Feng, Y.-X., Suwargadi, B.W., 2010. Evidence for Holocene changes in Australian–Indonesian monsoon rainfall from stalagmite trace element and stable isotope ratios. Earth Planet. Sci. Lett. 292, 27–38.
Grimm, E.C., 1993. Tilia. Illinois State Museum, Springfield, IL.
Grimm, E.C., 2004. TGView. Illinois State Museum, Springfield, IL.
Gupta, A.K., Das, M., Anderson, D.M., 2005. Solar influence on the Indian summer monsoon during the Holocene. Geophys. Res. Lett. 32, L17703. http://dx.doi.org/10.1029/2005GL022685.
Haug, G.H., Hughen, K.A., Peterson, L.C., Sigman, D.M., Röhl, U., 2001. Southward migration of the Intertropical Convergence Zone through the Holocene. Science 293, 1304–1308.
Heaton, T.H.E., Holmes, J.A., Bridgwater, N.D., 1995. Carbon and oxygen isotope variations among lacustrine ostracods: implications for palaeoclimatic studies. Holocene 5, 428–434.
Krammer, K., Lange-Bertalot, H., 1999. Bacillariophyceae 1 & 2. In: Susswasserflora von Mittleuropa, vol. 2. Fischer, Jena, Stuttgart, Germany.
MacDonald, G., 2011. Potential influence of the Pacific Ocean on the Indian summer monsoon and Harappan decline. Quat. Int. 229, 140–148.
Marchant, R.A., Hooghiemstra, H., 2004. Rapid environmental change in tropical Africa and Latin America about 4000 years before present: a review. Earth-Sci. Rev. 66, 217–260.
Marchant, R., Mumbi, C., Behera, S., Yamagata, T., 2006. The Indian Ocean dipole – the unsung driver of climatic variability in East Africa. Afr. J. Ecol. 45, 4–16.
Mayer, L.M., Schick, L.L., Allison, M.A., Ruttenberg, K.C., Bentley, S.J., 2007. Marine vs. terrigenous organic matter in Louisiana coastal sediments: the uses of bromine: organic carbon ratios. Mar. Chem. 107, 244–254.
McCormac, F.G., Hogg, A.G., Blackwell, P.G., Buck, C.E., Higham, T.F.G., Reimer, P.J., 2004. SHCal04 Southern Hemisphere calibration 0–11.0 cal kyr BP. Radiocarbon 46, 1087–1092.
Moy, C.M., Seltzer, G.O., Rodbell, D.T., Anderson, D.M., 2002. Variability of El Niño/Southern Oscillation activity at millennial timescales during the Holocene epoch. Nature 420, 162–165.
North, S.G., Bullock, D.J., 1986. Changes in the vegetation and populations of introduced mammals of Round Island and Gunner's Quoin, Mauritius. Biol. Conserv. 37, 99–117.
Oude Essink, G.H.P., 1996. Impact of Sea Level Rise on Groundwater Flow Regimes. A Sensitivity Analysis for the Netherlands (Ph.D. thesis). Delft University of Technology. Delft Studies in Integrated Water Management, p. 428.
Padya, B.M., 1989. Weather and Climate of Mauritius. In: Geography of Mauritius Series. Mahatma Gandhi Institute Press/Mahatma Gandhi Institute, Moka.
Partin, J.W., Cobb, K.M., Adkins, J.F., Clark, B., Fernandez, D.P., 2007. Millennial-scale trends in west Pacific warm pool hydrology since the Last Glacial Maximum. Nature 449, 452–455.
Patrick, R., Reimer, C., 1966. The Diatoms of the United States. Monographs of the Academy Natural Science, Philadelphia, 13(1): 688 pp, and 13(2): 213 pp.
Richter, T.O., Van der Gaast, S., Koster, B., Vaars, A., Gieles, R., de Stigter, H.C., de Haas, H., van Weering, T.C.E., 2006. The Avaatech core scanner: technical description and applications to NE Atlantic sediments. In: Rothwell, R.G. (Ed.), New Ways of Looking at Sediment Core and Core Data, Geological Society Special Publication, vol. 267, pp. 39–50.
Rijsdijk, K.F., Zinke, J., De Louw, P.G.B., Hume, J.P., Van der Plicht, J., Hooghiemstra, H., Meijer, H.J.M., Vonhof, H.B., Porch, N., Florens, F.B.V., Baider, C., Van Geel, B., Brinkkemper, J., Vernimmen, T., Janoo, A., 2011. Mid-Holocene (4200 yr) mass mortalities in Mauritius (Mascarenes): insular vertebrates resilient to climatic extremes but vulnerable to human impact. Holocene 21, 1179–1194.
Rohling, E.J., Liu, Q.S., Roberts, A.P., Stanford, J.D., Rasmussen, S.O., Langen, P.L., Siddall, M., 2009. Controls on the East Asian monsoon during the Last Glacial cycle, based on comparison between Hulu Cave and polar ice-core records. Quat. Sci. Rev. 28, 3291–3302.
Saddul, P., 2002. Mauritius: a Geomorphological Analysis. Mahatma Gandhi Institute, Mauritius, p. 354.
Safford, R.J., 1997. A survey of the occurrence of native vegetation remnants on Mauritius in 1993. Biol. Conserv. 80, 181–188.
Saji, N.H., Goswami, B.N., Vinayachandran, P.N., Yamagata, T., 1999. A dipole mode in the tropical Indian Ocean. Nature 401, 360–363.
Sala, S., Duque, S., Nuñez-Avellaneda, M., Lamaro, A., 2002. Diatoms from the Colombian Amazonia. Cryptogam. Algol. 23, 75–99.
Schott, F.A., McCreary Jr., J.P., 2001. The monsoon circulation of the Indian Ocean. Prog. Oceanogr. 51, 1–123.
Schott, F.A., Xie, S.-P., McCreary Jr., J.P., 2009. Indian Ocean circulation and climate variability. Rev. Geophys. 47, RG1002. http://dx.doi.org/10.1029/2007RG000245.
Schefuß, E., Kuhlmann, H., Mollenhauer, G., Prange, M., Pätzold, J., 2011. Forcing of wet phases in southeast Africa over the past 17,000 years. Nature 480, 509–512.
Senapathi, D., Underwood, F., Black, E., Nicoll, M.A.C., Norris, K., 2010. Evidence for long-term regional changes in precipitation on the East Coast Mountains in Mauritius. Int. J. Climatol. 30, 1164–1177.
Staubwasser, M., Sirocko, F., Grootes, P.M., Segl, M., 2003. Climate change at the 4.2 ka BP termination of the Indus valley civilization and Holocene south Asian monsoon variability. Geophys. Res. Lett. 30. http://dx.doi.org/10.1029/2002GL016822.
Stott, L., Cannariato, K., Thunell, R., Haug, G.H., Koutavas, A., Lund, S., 2004. Decline of surface temperature and salinity in the western tropical Pacific Ocean in the Holocene epoch. Nature 431, 56–59.
Sylvestre, F., Servant-Vildary, S., Roux, M., 2001. Diatom-based ionic concentration and salinity models from the South Bolivian Altiplano (15-23°S). J. Paleolimnol. 25, 279–295.
Thomas, D.S.G., Bailey, R., Shaw, P.A., Durcan, J.A., Singarayer, J.S., 2009. Late Quaternary highstands at Lake Chilwa, Malawi: frequency, timing and possible forcing mechanisms in the last 44 ka. Quat. Sci. Rev. 28, 526–539.
Tierney, J.E., Russell, J.M., Huang, Y., Sinninghe Damsté, J.S., Hopmans, E.C., Cohen, A.S., 2008. Northern Hemisphere controls on tropical southeast African climate during the past 60,000 years. Science 322, 252–255.
Tierney, J.E., Russell, J.M., Sinninghe Damsté, J.S., Huang, Y., Verschuren, D., 2011. Late Quaternary behavior of the East African monsoon and the importance of the Congo Air Boundary. Quat. Sci. Rev. 30, 798–807.
Tjallingii, R., Röhl, U., Kölling, M., Bickert, T., 2007. Influence of the water content on X-ray fluorescence core-scanning measurements in soft marine sediments. Geochem. Geophys. Geosyst. 8, Q02004. http://dx.doi.org/10.1029/2006GC001393.
Thompson, L.G., Mosley-Thompson, E., Davis, M.E., Henderson, K.A., Brecher, H.H., Zagorodnov, V.S., Mashiotta, T.A., Lin, P.-N., Mikhalenko, V.N., Hardy, D.R., Beer, J., 2002. Kilimanjaro ice core records: evidence of Holocene climate change in tropical Africa. Science 298, 589–593.
Toth, L.T., Aronson, R.B., Vollmer, S.V., Hobbs, J.W., Urrego, D.H., Cheng, H., Enochs, I.C., Combosch, D.J., Van Woesik, R., Macintyre, I.G., 2012. ENSO drove 2500-year collapse of Eastern Pacific coral reefs. Science 337, 81–84.
Van der Plas, G.W., De Boer, E.J., Hooghiemstra, H., Florens, F.B.V., Baider, C., Van der Plicht, J., 2012. Mauritius since the Last Glacial: environmental and climatic reconstruction of the last 38,000 years from Kanaka Crater. J. Quat. Sci. 7, 159–168.
Van Rampelbergh, M., Fleitmann, D., Verheyden, S., Cheng, H., Edwards, L., De Geest, P., De Vleeschouwer, D., Burns, S.J., Matter, A., Claeys, P., Keppens, E., 2013. Mid- to late Holocene Indian Ocean monsoon variability recorded in four speleothems from Socotra Island, Yemen. Quat. Sci. Rev. 65, 129–142.
Vaughan, R.E., Wiehe, P.O., 1937. Studies on the vegetation of Mauritius: a preliminary survey of the plant communities. J. Ecol. 25, 289–343.
Verschuren, D., Sinninghe Damsté, J.S., Moernout, J., Kristen, I., Blaauw, M., Fagot, M., Haug, G.H., CHALLACEA Project Members, 2009. Half-precessional dynamics of monsoon rainfall near the East African equator. Nature 462, 637–641.
Vincens, A., Chalié, F., Bonnefille, R., 1993. Pollen-derived rainfall and temperature estimates from lake Tanganyika and their implication for Late Pleistocene water levels. Quat. Res. 40, 343–350.
Vincens, A., Buchet, G., Williamson, D., Taieb, M., 2005. A 23,000 yr pollen record from Lake Rukwa (8°S, SW Tanzania): new data on vegetation dynamics and climate in Central Eastern Africa. Rev. Palaeobot. Palynol. 137, 147–162.
Virah-Sawmy, M., Willis, K.J., Gillson, L., 2010. Evidence for drought and forest declines during the recent megafaunal extinctions in Madagascar. J. Biogeogr. 37, 506–519.
Wang, Y., Cheng, H., Lawrence Edwards, R., He, Y., Kong, X., An, Z., Wu, J., Kelly, M.J., Dykoski, C.A., Li, X., 2005. The Holocene Asian monsoon: links to solar changes and North Atlantic climate. Science 308, 854–857.
Weltje, G.J., Tjallingii, R., 2008. Calibration of XRF core scanners for quantitative geochemical logging of soft sediment cores: theory and application. Earth Planet. Sci. Lett. 274, 423–438.
Witkowski, A., Lange-Bertalot, H., Metzeltin, D., 2000. Diatom Flora of Marine Coasts I. In: Iconographia Diatomologica, vol. 7. Königstein: Koeltz Scientific Books.
Ziegler, M., Jilbert, T., de Lange, G.J., Lourens, L.J., Reichart, G.-J., 2008. Bromine counts from XRF scanning as an estimate of the marine organic carbon content of sediment cores. Geochem. Geophys. Geosyst. 9, Q05009. http://dx.doi.org/10.1029/2007GC001932.